Hydrodynamic spinning of protein fractal aggregates into core-shell fibers

Alice Vilotte, Clément de Loubens, Deniz Gunes, Christophe Schmitt, Hugues Bodiguel

Hydrodynamic spinning of protein fractal aggregates into core-shell fibers

Alice Vilotte,[†] Clément de Loubens,[*,†] Deniz Z. Gunes,[‡,¶] Christophe Schmitt,[‡] and Hugues Bodiguel[†]

[†]*Univ. Grenoble Alpes, CNRS, Grenoble INP, LRP, 38000 Grenoble, France*
[‡]*Nestlé Research, Nestlé Institute of Material Sciences, Vers-Chez-Les-Blanc, Lausanne, CH-1000 26, Switzerland*
[¶]*Present address: Department of Chemical Engineering and Center for Food and Microbial Technology, KU Leuven, 3001 Leuven, Belgium*

E-mail: clement.de-loubens@univ-grenoble-alpes.fr

Abstract

Using fractal protein aggregates as building blocks, porous fibers were produced. The suspension of aggregates was co-injected with a solution of calcium chloride. Sol-gel transition of the suspension was induced by diffusion of calcium ions in the jet. The production of these fibers required a precise control of both hydrodynamic and physicochemical conditions as hydrodynamic instabilities competed with the gelation kinetics. By increasing the calcium concentration, several regimes were observed: swollen, dispersed and shrunk fibers. In the first regime, homogeneous fibers were obtained. In the last one, osmotic phenomena led to a spontaneous core-shell structure with a dense shell.

Keywords

cold gelation, calcium, whey protein isolate, osmotic flow, microfluidics, food

Hydrogel microfibers have attracted interest in a wide range of fields: bio-engineering,[1] food science[2] or microelectronics.[3] The high surface-to-volume ratio of fibers makes them an asset for tailoring the rheological properties of suspensions[4] and for the controlled release of molecules.[5] Nature also offers examples of protein-based fibers with unique mechanical strength.[6] The control of fiber morphology also opens up new perspectives in term of applications.[7] For example, alginate core-shell fibers were used as scaffold for cells[1] or for the design of flexible electronic systems.[3] Lipid digestion was also controlled by encapsulation of lipid in biopolymers fibers.[2]

By taking advantage of the control of multilaminar flows, microfluidics is becoming the method of choice for producing fibers with controlled shapes.[7] For example, the production of hollow fibers is generally achieved by the coinjection of at least three different phases.[8] The inner phase contains the compound to be encapsulated in the core; the middle phase contains the biopolymer and the external phase contains the cross-linker which diffuses to form the shell.[9] However, these multi-phase reactive flows of complex fluids are prone to hydrodynamic instabilities,,[10–12] which makes them difficult to scale-up.

To control not only the shape but also the structure of the fibers, protein-based colloidal objects were also used as a building block.[7] Indeed, proteins can form colloidal objects with various structures depending on the physicochemical conditions of aggregation. Nanofibrils of proteins were oriented inside the fibers using microfluidic technologies.[7,13,14] Their ori-

entation and entanglement enabled modulation of the mechanical strength of the fiber.[15] Here, we went a step further in the formation of protein-based fibers with a hierarchical structure by using sub-micrometric fractal aggregates as the building block. The interest of using fractal aggregates instead of homogeneous particles lies in the fact that their density ρ decreases as their size R increases, as $\rho \propto R^{d_f-3}$ where d_f is the fractal dimension. Since, size, fractal dimension and density of aggregates are controllable,[16,17] it should be possible to tune the physical properties of such fibers (density, elasticity), if these sub-micrometric aggregates can be assemble into micrometric fibers.

In this Letter, we focused on the spinning of edible whey protein isolate (WPI) derived from cow's milk which is mainly composed of two globular proteins, β-lactoglobulin and α-lactabulmin. At temperatures higher than 65-70°C, proteins lose their native structure and form aggregates. Depending on the balance between repulsive and attractive forces, nanofibrils, microgels or fractal aggregates are obtained by changing the pH from 2.0 to 7.0 and adjusting the ionic strength.[16,18] Using fractal aggregates as building blocks, we produced porous fibers. Gelation was triggered by the addition of calcium chloride[19] in a core-annular flow. Although this process was simple, obtaining porous fibers required a precise control of both hydrodynamic and physicochemical conditions. Surprisingly, these fibers spontaneously exhibited a core-shell structure, triggered by osmotic phenomena.

The suspension of fractal aggregates was obtained by heat-induced denaturation and aggregation at 92°C for 30 min of a solution of WPI (17.5×10^3 g/mol) at pH 7.0. The initial dispersion used to produce fibers just below the sol-gel transition, i.e. 8 wt% WPI at 10 mM NaCl (Fig. 1-a). These conditions led to the formation of aggregates[17] with a fractal dimension of about 2 and a hydrodynamic radius R_h of 70 nm, as measured by dynamic light scattering (Vasco Cordouan Technologies, λ=658 nm). The concentration of the aggregates, C_{agg}, was then varied from 6.6 to 10.1 wt%, either by dilution or by gentle evaporation at 30°C for several hours. The viscosity of these suspensions was measured using standard rheometry and increased exponentially from 6.9 to 38 mPa.s when the concentration of the aggregates was increased from 6.6 to 10.1 wt%, in agreement with Ref.[20] By adding calcium chloride at room temperature, the suspensions of aggregates gelled for calcium concentrations higher than 5 mM. It resulted from both screening of electrostatic interactions and specific binding of calcium ions to the aggregates. Above 30 mM, syneresis was observed.[21]

As depicted in Fig. 1-b, the shaping of continuous gelled fibers requires two key steps: hydrodynamic spinning with a core-annular flow between the suspension of aggregates (inner phase) and a solution of calcium chloride (outer phase); maturation of the fibers in a bath of a calcium chloride solution at the same concentration as that used for the outer flow. This concentration ranged from 35 mM to 5.9 M and is expressed as a molar ratio, R_m, between calcium ions and WPI (R_m = 7.8 - 1560).

The core-annular flow was established by a coaxial needle (Ramé-Hart Instruments), with inner and outer radii r_i = 178 μm and r_o = 356 μm, respectively. A syringe pump (Nemesys, Cetoni) was used to control the core and annular flow rates, Q_{agg} and $Q_{\text{Ca}^{2+}}$. The needle was embedded into a fluorinated ethylene-propylene flexible tube (Fluigent) immersed in a water-bath (27°C). The tube length L was adjusted from 11 to 225 cm in order to keep the residence time $\tau_r = L/v$ unchanged when flow rates were varied, where $v = (Q_{\text{agg}} + Q_{\text{Ca}^{2+}})/\pi r_o^2$ is the mean velocity. To avoid long tube length, τ_r was set to 6 s, which was almost two orders of magnitude lower than the characteristic time of calcium ions diffusion in the core of the flow $\tau_d \simeq r_i^2/D \simeq$ 300-500 s. However this short first step was sufficient to stabilize the fiber by ionic cross-linking of the aggregates at the periphery of the inner jet, Fig 1-e. In order to induce a complete gelation of the fibers, they were stored for 20 min in a calcium bath, Fig 1-b, f. Afterwards, a suspension of fibers with diameter of 100 μm and a few centimeters in length, was obtained, Fig 1-c. Fig 1-d shows a fiber that was strained up to 100 %

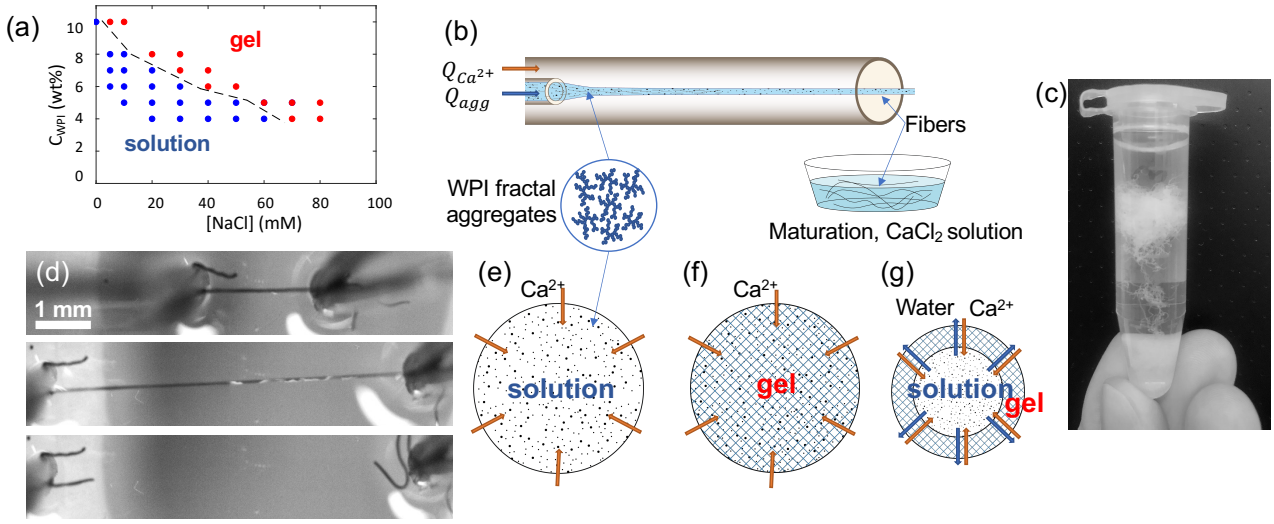

Figure 1: **a:** Sol-gel diagram of suspensions of fractal WPI aggregates obtained by heating at 92°C and for 30 min a solution of WPI at pH 7.0. **b:** Solutions of fractal aggregates were spun in a core-annular flow with a solution of $CaCl_2$ to initiate the sol-gel transition at the periphery of the fiber. During the maturation step, fibers were kept for 20 min in a solution of $CaCl_2$ to completely gel the fibers. **c:** Photograph of WPI aggregate fibers. d: Snapshots of a fiber being manually stretched up to break-up. Scale-bar 1 mm. e-g: Fibers were gelled by diffusion and ionic cross-linking of Ca^{2+}. **f:** At low ionic strength, the gelation was uniform in the fibers. **g:** At high ionic strength, an osmotic water flux from the fiber to the $CaCl_2$ solution concentrated the aggregates at the periphery of the fiber and spontaneously generated a core-shell structure.

of its initial length before break-up. Images of the gelled fibers were systematically taken by bright field microscopy (Olympus IX-72) with a ×4 objective just after the production, and all along the maturation step.

We will first consider results on the role concerning the role of the hydrodynamic parameters. Depending on the flow rates, either long fibers or some pieces of gel were observed at the outlet of the tube (see examples displayed in Fig. 2-b). The state diagram of fiber formation (Fig. 2-a) shows that fibers were only obtained in a narrow range of mean velocity, $v_1 < v < v_2$, for a given flow rate ratio $q = Q_{\mathrm{Ca^{2+}}}/Q_{\mathrm{agg}}$. When q was increased, the fiber diameter decreased but the range of existence was reduced further as v_1 increased and v_2 decreased simultaneously.

In core-annular laminar flows of Newtonian fluids, and after an entrance region of the order of a few tube diameters, the diameter D of the inner phase is predicted by solving momentum balance and mass conservation equations.[11] It reads $D = 2r_o\left[(\alpha-1)/(\alpha-1+m)\right]^{1/2}$, where m is the viscosity ratio $m = \eta_{Ca^{2+}}/\eta_{agg}$ and $\alpha = \sqrt{1+m/q}$. Since we focused on regimes where $q > 1$ and $m \ll 1$, $\alpha \approx 1$, and the diameter could be more simply expressed as $D = 2r_0/\sqrt{1+2q}$. In Fig. 2-c, this prediction is plotted together with the experimental data as a function of q, and for several molar ratio R_m. A good quantitative agreement was found. This was expected since the diffusion of the protein aggregates was negligible. Note that a small but significant decrease of the diameter was observed when the calcium concentration was increased. This point will be discussed, further in this paper.

The two critical velocities $v_1(q)$ and $v_2(q)$ likely have two different physical origins.

For $v < v_1$, direct observation at the inlet of the tube revealed the formation of a clog on the needle that was regularly evacuated. By introducing a characteristic gelation time τ_g, we can tentatively write that a plug is formed when the distance travelled by the aggregates during τ_g is smaller than the entrance region ($\simeq r_o$), i.e. when $\tau_g < r_o^3/Q_{agg}$. This condition is equivalent

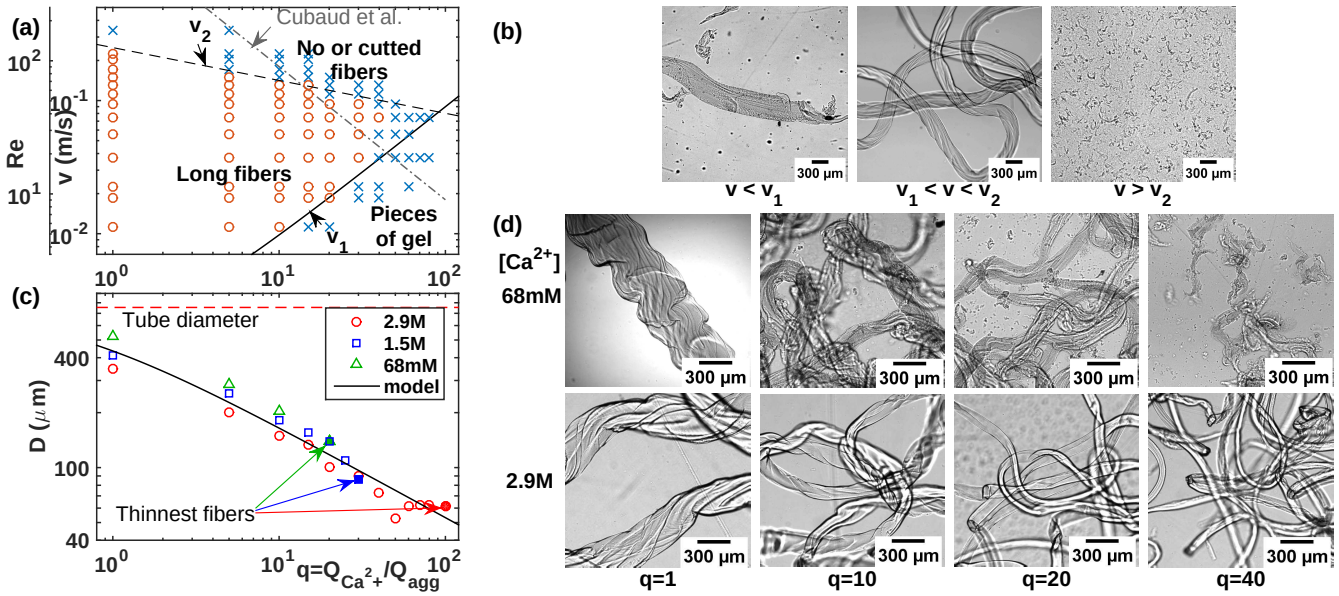

Figure 2: **a:** State diagram of fiber production in the $v-q$ plane, for $C_{\rm agg}=8\%$, $t=6$ s and $\mathrm{Ca}^{2+}=1.5$M. The dashed line is a guide-for the eye corresponding to the high velocity limit v_2. Solid line is the v_1 criterion given by $r_0(1+q)/\tau_g$ with $\tau_g=0.4$ s (see text). The dash-dotted line is the inertial instability threshold determined in Cubaud and Notaro[12]. **b:** Image examples of the three regimes. Experimental conditions are (from left to right): $v=0.018$, 0.0739, and 0.3359 m/s; $q=40$, 10 and 5. **c:** Fiber diameter measured just after the production, for $v=7.5\times10^{-2}$ m/s, $C_{\rm agg}=8\%$ and $t=6$ s. For each calcium chloride concentration, the thinnest fiber produced is highlighted using a full symbol. At higher q, the fibers were cut into small pieces. The solid line is the model prediction, $D=2r_o\,(1+2q)^{-1/2}$. **d:** Examples of fiber images obtained using bright field microscopy.

to $v<v_1$, where $v_1=r_o\,(q+1)\,/\tau_g$. It provides a good description of the low-velocity limit of the diagram with $\tau_g=0.4$ s (Fig. 2-a, plain line). This characteristic time is consistent with the fact that a droplet of WPI dropped in 1.5 M $CaCl_2$ solution gelled almost instantaneously.

Conversely, the high velocity limit, v_2, is likely to arise from flow instabilities, which are common in core-annular flows of miscible fluids.[22] Thread destabilization is triggered by diffusion or inertia depending on the Péclet (Pe) and Reynolds numbers (Re).[12] Our experiments were carried out in flow conditions which were stable with respect to diffusive instabilities, since $\mathrm{Pe}=vr_o/D_{Ca^{2+}}$ ranged from 0.5 to 10×10^4, whereas diffusive instabilities are triggered for Pe smaller than $\simeq0.5\times10^4$.[12] Inertia-driven instabilities were observed for miscible (and non-reactive) fluids above a critical value of Reynolds number $\mathrm{Re}_c=900/q$ for a viscosity ratio of 10^{12} (Fig. 2-a, dashed-dotted line). The order of magnitude of Re_c matches the high velocity limit v_2, especially for $q>10$. A discrepancy is found at lower q, and the scaling is not consistent, since we found $v_2\sim q^{-0.5}$. This apparent disagreement might originate from the fact that in the work of Cubaud and Notaro,[12] the investigated range of q was typically 10-1000. Other experimental or theoretical work have also been reported on miscible core-annular flow instabilities,[23–25] but only scarce data as a function of q are available, in particular for the viscosity ratio range considered in this Letter. Therefore, it seems difficult to draw conclusions concerning the low-q regime (q<10), but the qualitative agreement found at higher q with the work of Cubaud and Notaro supports the idea that the v_2 limit of fiber formation was due to inertial hydrodynamic instabilities.

Since cold-set gelation of WPI is a slow and complex process (the shear modulus of the gel

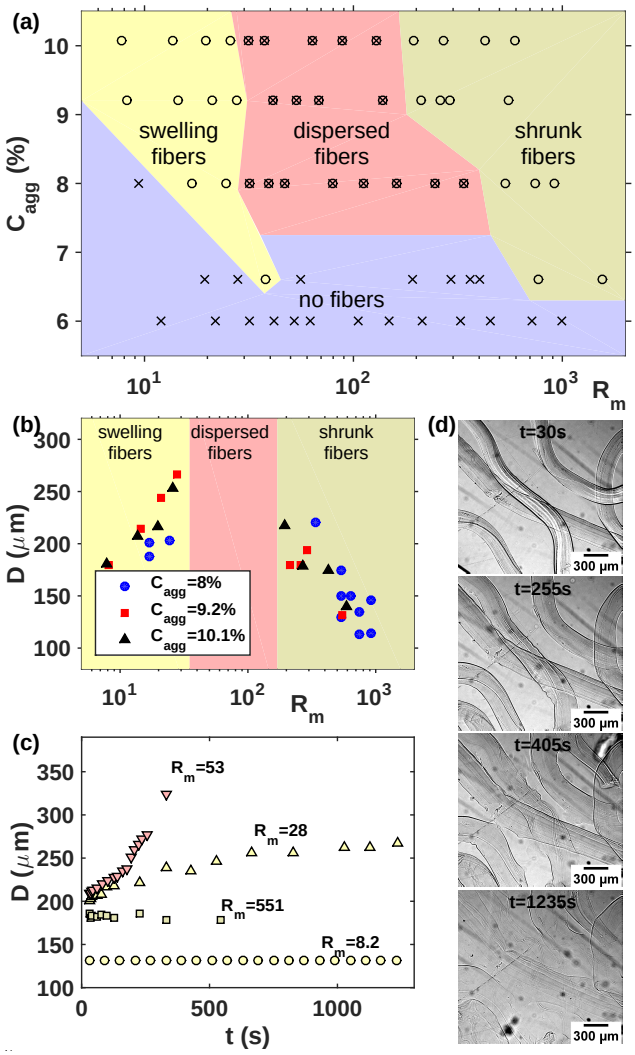

Figure 3: **a:** State diagram of fiber formation and maturation for various calcium concentrations (converted in molar ratio R_m) and injected protein aggregate concentration C_{agg}. Flow conditions were $v = 7.4 \times 10^{-2}$ m/s and $q = 10$. Circles stand for stable fibers within 20 min of maturation step. Crossed circles for cases where a fiber was initially formed but then was dispersed during the maturation step. Crosses are for cases where no fibers were formed. **b:** Final fiber diameters (after 20 min maturation). **c:** Examples of fiber diameter measured during the maturation step and plotted as a function of time ($C_{\text{agg}} = 9.2\%$). **d:** image sequence during the maturation step in the dispersed fibers regime ($R_m = 53$, $C_{\text{agg}} = 9.2\%$).

increases slowly over several decades in time[21]) and the residence time is short compared to the time of Ca^{2+} diffusion, a maturation step was required to consolidate the fibers.

We observed rather complex phenomena during this maturation step, summarized in Fig. 3-a.

At low calcium chloride concentration (e.g. $R_m = 28$), the fibers tended to swell (Fig. 3-c). In contrast, the diameter of the fibers produced at very high calcium concentration remained steady. In these two regimes, as cross-linking by calcium ions is irreversible, fibers could be stored during several days without any significant change in size or strength. More surprisingly, in between these two regimes (e.g. $R_m = 53$), we observed that the fibers eventually broke up and dispersed after being swollen (Fig. 3-c,d). We were not able to produce fibers at protein concentrations below 6 wt%, Fig. 3-A. At 8 wt% and above, the three regimes were systematically observed. Final diameters of the fibers were roughly independent of protein concentration (Fig. 3-b). In the swelling regime, the final diameter increased from 180 μm up to 260 μm when the calcium concentration was increased. In the stable regime, a rather strong decrease of the diameter was observed when the calcium concentration was further increased, suggesting a shrinkage occurring during the production step.

These observations are puzzling since the increase of the calcium concentration led successively to a swelling, then to a dispersion, and finally to a shrinkage of the fibers. Such a non-monotonic behavior was reported for calcium-induced gelation of whey proteins:[26] both the gelation rate and the Young's modulus of the gel exhibited a maximum when the calcium concentration was increased.[26,27] Concomitantly, the fractal dimension of the aggregates was seen to increase. This phenomenon might result from a balance between inter- and intra-aggregate bridging by the calcium ions, the latter being dominant at high concentration. This led to a micro-phase separation, as the density of the aggregates increased due to intra-aggregate bridging of carboxylate groups. Similar behavior was reported in globular protein/polyelectrolyte mixtures as a function of the charge neutralisation ratio.[28]

One macroscopic consequence of this phe-

nomenon is syneresis, which is observed in gels at high calcium concentration.[21] It can explain both the swelling and the dispersion of the fibers observed during the maturation step. Indeed, swelling or dispersion of the fibers were rather slow, typically 10^3 s, an order of magnitude which coincides with the diffusion time of the aggregates over the fiber radius, $\tau_d \sim r^2/D_{agg} \sim 8 \times 10^2$ s with $r \sim 50$ μm and $D_{agg} \sim 3 \times 10^{-12}$ m^2/s. The range in calcium concentration where fiber dispersion occurred (typically 100 mM) was also compatible with the onset of macroscopic syneresis[21] (30 mM) for similar initial protein aggregates.

The shrinkage regime observed at even higher calcium concentration remains to be elucidated as it does not match this physical picture. Indeed, shrinkage occurred during the 6 s of the production step.

An additional physical phenomenon must therefore be considered. In a forthcoming communication, we proved that gelled biopolymers such as WPI or alginate very partially act as a semi-permeable membrane.we proved that gelled biopolymers such as WPI or alginate very partially act as a semi-permeable membrane. The consequence of this behaviour is the spontaneous generation of an osmotic flux from the solution of biopolymer towards the solution of calcium through the gel at high osmotic pressure difference. This osmotic flux tends to concentrate the aggregates in the gel under formation. Transposing this osmotic flow in the case of fibers, one can expect, as observed, a shrinkage of the fibers, together with an increase of the protein concentration at its periphery, as shown in Figure 1-g.

To check this assumption, electronic (SEM) and confocal fluorescence microscopy (Leica TCS SP8) were used. The apparent porosity seen on SEM images was due to freeze-drying (Fig. 4-a,b, see Supp. Mat.). Fibers produced in the low calcium concentration regime exhibited a uniform inner structure (Fig. 4-a). In contrast, those obtained in the high concentration regime showed a dense shell surrounding a core (Fig. 4-b). This core-shell structure of the shrunk fibers was further confirmed more quantitatively using confocal microscopy by imaging the fibers mid-plane Fig. 4-c,d. As WPI were labelled with a fluorescent dye,[29] the fluorescent intensity is approximately proportional to the protein concentration. The shrunk fibers exhibited an intensity gradient along the radial direction, whereas the fluorescent intensity was constant for the fibers produced at low calcium concentration (Fig. 4-d). The excess protein concentration in the shell was about 20% for the shrunk fibers. This order of magnitude might appear moderate, but it represents a significant increase in terms of mechanical properties[21]. These observations are consistent with the scenario proposed above: an osmotic flow occurred from the inside to the periphery of the fiber, leading to an increase of the aggregate concentration in the shell, and a decrease of its radius.

In conclusion, fibers made of whey protein aggregates were shaped by hydrodynamic spinning. Fiber diameter was simply tuned by the hydrodynamic conditions. The velocity range where long and uniform fibers could be produced, was relatively narrow because the velocity needed to be sufficiently high to delay gelation near the inlet, and sufficiently low to prevent hydrodynamic instabilities. The concentration of calcium ions had important consequences. At low concentrations, fibers with uniform inner structure were produced. Then, fibers were not stable. At very high calcium concentrations, fibers shrunk and exhibited a dense shell. Although the intermediate regime is probably specific to the particular interaction between the whey proteins and the calcium ions, the concentration gradient observed in the high concentration regime is likely to be generic to other systems. It was interpreted as a consequence of an osmotic flow taking place from the inside to the outside of the fiber. The possibility of obtaining a composition gradient or a core-shell structure spontaneously paves the way to controlling the structure of fibers or microparticles made of colloidal particles.

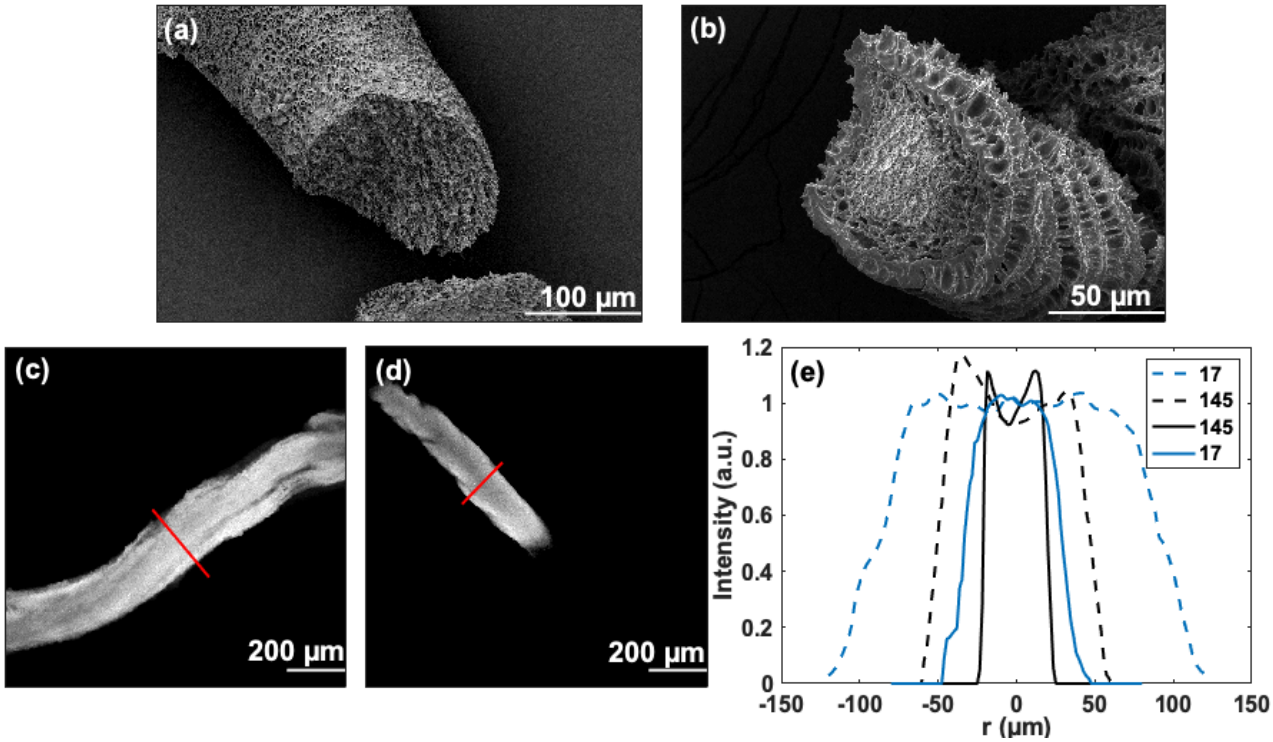

Figure 4: Imaging of freeze-dried fibers by scanning electron microscopy at low (**a**, $R_m = 17$) and high (**b**, $R_m = 145$) calcium concentrations. The apparent porosity was due to freeze-drying. Confocal scanning microscopy of the mid-plane of fibers made of WPI labelled with a fluorescent in distilled water at low (**c**, $R_m = 17$) and high (**d**, $R_m = 145$) molar ratios. **e:** Fluorescent intensity profile along the radial direction r of the fiber (red lines) at high and low molar ratios and for fibers of different diameters. For each sample, the fluorescent intensity is an averaged over 4-5 cross-sections and was rescaled by the mean intensity.

Supporting Information Available

A table of the notations and a description of the experimental procedure for scanning-electron microscopy are given in supplementary material.

Acknowledgement LRP is part of the LabEx Tec21 (ANR-11-LABX-0030) and of the PolyNat Carnot Institute (ANR-11-CARN-007-01). The authors thank Christine Lancelon-Pin (CERMAV-CNRS, Grenoble, France) for her assistance with scanning-electron microscopy. The authors acknowledge the NanoBio-ICMG chemistry platform (UAR 2607, Grenoble) for granting access to the electron microscopy facilities.

References

(1) Andrique, L.; Recher, G.; Alessandri, K.; Pujol, N.; Feyeux, M.; Bon, P.; Cognet, L.; Nassoy, P.; Bikfalvi, A. A model of guided cell self-organization for rapid and spontaneous formation of functional vessels. *Science advances* **2019**, *5*, eaau6562.

(2) Sordo, F.; Janecek, E.-R.; Qu, Y.; Michaud, V.; Stellacci, F.; Engmann, J.; Wooster, T. J.; Sorin, F. Microstructured fibers for the production of food. *Advanced Materials* **2019**, *31*, 1807282.

(3) Guo, J.; Yu, Y.; Wang, H.; Zhang, H.; Zhang, X.; Zhao, Y. Conductive polymer hydrogel microfibers from multiflow microfluidics. *Small* **2019**, *15*, 1805162.

(4) Zirnsak, M.; Hur, D.; Boger, D. Normal stresses in fibre suspensions. *Journal of*

non-newtonian fluid mechanics **1994**, *54*, 153–193.

(5) Singh, A.; Rath, G.; Singh, R.; Goyal, A. K. Nanofibers: An effective tool for controlled and sustained drug delivery. *Current drug delivery* **2018**, *15*, 155–166.

(6) Rammensee, S.; Slotta, U.; Scheibel, T.; Bausch, A. R. Assembly mechanism of recombinant spider silk proteins. *Proceedings of the National Academy of Sciences* **2008**, *105*, 6590–6595.

(7) Wu, R.; Kim, T. Review of microfluidic approaches for fabricating intelligent fiber devices: importance of shape characteristics. *Lab on a Chip* **2021**, *21*, 1217–1240.

(8) Naeimirad, M.; Zadhoush, A.; Kotek, R.; Esmaeely Neisiany, R.; Nouri Khorasani, S.; Ramakrishna, S. Recent advances in core/shell bicomponent fibers and nanofibers: A review. *Journal of Applied Polymer Science* **2018**, *135*, 46265.

(9) Shin, S.-J.; Park, J.-Y.; Lee, J.-Y.; Park, H.; Park, Y.-D.; Lee, K.-B.; Whang, C.-M.; Lee, S.-H. "On the fly" continuous generation of alginate fibers using a microfluidic device. *Langmuir* **2007**, *23*, 9104–9108.

(10) Williams, H.; McPhail, M.; Mondal, S.; Münch, A. Modeling gel fiber formation in an emerging coaxial flow from a nozzle. *Journal of Fluids Engineering* **2019**, *141*.

(11) Bonhomme, O.; Morozov, A.; Leng, J.; Colin, A. Elastic instability in stratified core annular flow. *Physical Review E* **2011**, *83*, 065301.

(12) Cubaud, T.; Notaro, S. Regimes of miscible fluid thread formation in microfluidic focusing sections. *Physics of Fluids* **2014**, *26*, 122005.

(13) Kamada, A.; Mittal, N.; Söderberg, L. D.; Ingverud, T.; Ohm, W.; Roth, S. V.; Lundell, F.; Lendel, C. Flow-assisted assembly of nanostructured protein microfibers. *Proceedings of the National Academy of Sciences* **2017**, *114*, 1232–1237.

(14) Lu, L.; Fan, S.; Niu, Q.; Peng, Q.; Geng, L.; Yang, G.; Shao, H.; Hsiao, B. S.; Zhang, Y. Strong silk fibers containing cellulose nanofibers generated by a bioinspired microfluidic chip. *ACS Sustainable Chemistry & Engineering* **2019**, *7*, 14765–14774.

(15) Kamada, A.; Levin, A.; Toprakcioglu, Z.; Shen, Y.; Lutz-Bueno, V.; Baumann, K. N.; Mohammadi, P.; Linder, M. B.; Mezzenga, R.; Knowles, T. P. Modulating the Mechanical Performance of Macroscale Fibers through Shear-Induced Alignment and Assembly of Protein Nanofibrils. *Small* **2020**, *16*, 1904190.

(16) Nicolai, T.; Britten, M.; Schmitt, C. β-Lactoglobulin and WPI aggregates: Formation, structure and applications. *Food Hydrocolloids* **2011**, *25*, 1945–1962.

(17) Vilotte, A.; Bodiguel, H.; Ako, K.; Gunes, D. Z.; Schmitt, C.; de Loubens, C. Kinetic and structural characterization of whey protein aggregation in a millifluidic continuous process. *Food Hydrocolloids* **2021**, *110*, 106137.

(18) Zuniga, R.; Tolkach, A.; Kulozik, U.; Aguilera, J. Kinetics of formation and physicochemical characterization of thermally-induced β-lactoglobulin aggregates. *Journal of Food Science* **2010**, *75*, E261–E268.

(19) Alting, A. C.; Hamer, R. J.; de Kruif, C. G.; Paques, M.; Visschers, R. W. Number of thiol groups rather than the size of the aggregates determines the hardness of cold set whey protein gels. *Food Hydrocolloids* **2003**, *17*, 469–479.

(20) Inthavong, W.; Kharlamova, A.; Chassenieux, C.; Nicolai, T. Structure and flow of dense suspensions of protein fractal aggregates in comparison with microgels. *Soft matter* **2016**, *12*, 2785–2793.

(21) Kharlamova, A.; Nicolai, T.; Chassenieux, C. Calcium-induced gelation of whey protein aggregates: Kinetics, structure and rheological properties. *Food Hydrocolloids* **2018**, *79*, 145–157.

(22) Govindarajan, R.; Sahu, K. C. Instabilities in viscosity-stratified flow. *Annual review of fluid mechanics* **2014**, *46*, 331–353.

(23) d'Olce, M.; Martin, J.; Rakotomalala, N.; Salin, D.; Talon, L. Pearl and mushroom instability patterns in two miscible fluids' core annular flows. *Physics of Fluids* **2008**, *20*, 024104.

(24) Martin, J.; Rakotomalala, N.; Salin, D.; Talon, L. Convective/absolute instability in miscible core-annular flow. Part 1: Experiments. *Journal of fluid mechanics* **2009**, *618*, 305–322.

(25) Salin, D.; Talon, L. Revisiting the linear stability analysis and absolute–convective transition of two fluid core annular flow. *Journal of Fluid Mechanics* **2019**, *865*, 743–761.

(26) Hongsprabhas, P.; Barbut, S.; Marangoni, A. The structure of cold-set whey protein isolate gels prepared with Ca++. *LWT-Food Science and Technology* **1999**, *32*, 196–202.

(27) Roefs, S.; Peppelman, H. Aggregation and gelation of whey proteins: specific effect of divalent cations. *Food colloids: Fundamentals of formulation* **2001**, 358e368.

(28) Gummel, J.; Boué, F.; Clemens, D.; Cousin, F. Finite size and inner structure controlled by electrostatic screening in globular complexes of proteins and polyelectrolytes. *Soft Matter* **2008**, *4*, 1653–1664.

(29) Schmitt, C.; Sanchez, C.; Lamprecht, A.; Renard, D.; Lehr, C.-M.; de Kruif, C. G.; Hardy, J. Study of β-lactoglobulin/acacia gum complex coacervation by diffusing-wave spectroscopy and confocal scanning laser microscopy. *Colloids and Surfaces B: Biointerfaces* **2001**, *20*, 267–280.

TOC Graphic

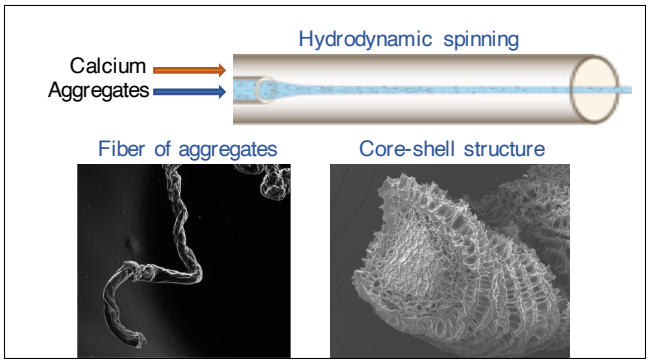
Hydrodynamic spinning
Calcium
Aggregates
Fiber of aggregates
Core-shell structure